
**Liquid Crystals**
Publication details, including instructions for authors and subscription information:
http://www.informaworld.com/smpp/title~content=t713926090

# Numerical analysis of the radial-axial structure transition with an applied field in a nematic droplet

S. Komura; R. J. Atkin; M. S. Stern; D. A. Dunmur

Online publication date: 06 August 2010

**To cite this Article** Komura, S. , Atkin, R. J. , Stern, M. S. and Dunmur, D. A.(1997) 'Numerical analysis of the radial-axial structure transition with an applied field in a nematic droplet', Liquid Crystals, 23: 2, 193 — 203
**To link to this Article: DOI:** 10.1080/026782997208442
**URL:** http://dx.doi.org/10.1080/026782997208442

LIQUID CRYSTALS, 1997, VOL. 23, NO. 2, 193–203

# Numerical analysis of the radial–axial structure transition with an applied field in a nematic droplet

by S. KOMURA*
Hitachi Research Laboratory, Hitachi Ltd., 1-1, Omika-cho 7-chome, Hitachi-shi, Ibaraki-ken, 319-12, Japan

R. J. ATKIN, M. S. STERN
School of Mathematics and Statistics, The University of Sheffield, Sheffield, S3 7HF, England

and D. A. DUNMUR
Department of Chemistry, The University of Sheffield, Sheffield, S3 7HF, England

(*Received 1 July 1996*)

In this paper the director configurations and the free energies of a nematic droplet with a surface normal anchoring condition are calculated numerically. For this surface anchoring, a transition occurs between the radial and axial structures with respect to an applied field. In the calculation of the director configurations, the position of a disclination has been fixed. Comparing the free energies for different disclinations, the stable position which gives the minimum free energy is found. In calculating the free energy of a droplet, it is assumed that the free energy density of the nematic phase does not exceed the isotropic free energy density, so that the large distortion in the vicinity of the disclination causes a nematic–isotropic transition and the free energy density of the disclination core becomes equal to the isotropic free energy density. The director configuration in a droplet is calculated as a function of an applied field for different isotropic free energy densities, elastic constant ratios and droplet shapes. The relation between the radial–axial structure transition and these factors are clarified.



## 1. Introduction

The change of director configurations with respect to an applied field in a nematic droplet is a matter of recent interest [1–6] in the context of polymer dispersed liquid crystals (PDLCs) [7–10]. Such materials containing nematic droplets are suitable for realising high brightness displays because they do not need any polarizers, unlike conventional liquid crystal displays. PDLCs consist of dispersed nematic droplets containing liquid crystals in a surrounding polymer, and by applying a voltage, PDLCs can be switched from a scattering state to a transparent state: this ability is especially suitable for projector applications [11–13].

In a nematic droplet, the director configuration depends on the anchoring condition at the droplet surface. In this paper, homeotropic anchoring where the directors prefer to align normal to the surface is assumed. Bondar *et al.* [3] observed experimentally the transition in a droplet with a homeotropic anchoring with respect to an applied field. They found that the radial structure with a point disclination at the centre of the droplet is stable without a field. With increasing an applied field, the disclination ring expands toward the surface and the axial structure with an equatorial disclination ring is stable at high field.

Kralj and Zumer [4] have analysed the radial–axial structural transition in a spherical droplet numerically. They considered the director configurations with a point disclination at the centre of the droplet, those with a disclination ring on the equatorial plane and those with an equatorial disclination ring on the surface and discussed the stability of these structures. They also discussed the dependencies of the structure on the ratio of elastic constants $K_{33}/K_{11}$, $K_{24}/K_{11}$, anchoring strength, and external field strength. Since the radial–axial structural transition is accompanied by the expansion of the disclination ring, which has a high free energy density, the free energy density of the disclination is very important. In this paper it is assumed that the core of the disclination is isotropic, and as an extension to the work of Kralj and Zumer, the dependence of

*Author for correspondence.

0267–8292/97 $12·00 

the radial–axial structural transition on the isotropic free energy density is discussed. Moreover the approach is extended to an oblate droplet and the director configuration in the oblate droplet is also considered.

The stable director configuration was obtained in the following way. Firstly the director configuration for the several possible positions of the disclination was calculated by solving the Euler–Lagrange equations numerically. In this calculation it was assumed that the director at the boundary surrounding the fixed disclination is given by solving the corresponding Euler–Lagrange equation around the disclination. Secondly the free energy in a droplet for each director configuration was calculated with a fixed disclination. Here it was assumed that the free energy density of the nematic phase does not exceed the isotropic free energy density [4]. The large distortion in the vicinity of the disclination causes a nematic–isotropic transition and the free energy density in the core of the disclination becomes equal to the isotropic free energy density. By comparing each free energy, the stable director configuration can be found by minimizing the free energy.

The director configurations of a spherical and an oblate droplet with homeotropic anchoring are calculated as a function of an applied electric field. Here the electric field is assumed to be constant in the droplet. The effects of the following factors on the radial-axial structure transition are discussed; (1) the difference between the isotropic free energy density and the nematic free energy density without distortion, (2) the elastic constant ratio $K_{33}/K_{11}$, (3) the difference between the oblate and spherical droplets.



## 2. Theory

The director configuration of a droplet is obtained by the condition of minimizing the free energy of a droplet. The free energy of a droplet is defined as

$$F = \iiint_v f_b \, dV + \iint_s f_s \, dS, \tag{1}$$

where $f_b$ and $f_s$ are the free energy density of the bulk and the surface, respectively. The bulk free energy density is the sum of the homogeneous term $f_n$, the distortion term $f_d$ and the external field term $f_e$ [4, 5] so that

$$f_b = f_n + f_d + f_e. \tag{2}$$

The homogeneous term means the free energy density of nematic phase without distortion and is a function of the order parameter.

In this paper only strong anchoring is considered. Surface terms in the Frank elastic free energy including $K_{13}$ and $K_{24}$ are neglected. Kralj and Zumer [4] also put $K_{13} = 0$ and found that $K_{24}$ was only significant for weak anchoring. Then the distortion term is given by

$$f_d = \frac{1}{2}K_{11}(\nabla \cdot \mathbf{n})^2 + \frac{1}{2}K_{22}[\mathbf{n} \cdot (\nabla \times \mathbf{n})]^2 + \frac{1}{2}K_{33}|\mathbf{n} \times (\nabla \times \mathbf{n})|^2, \tag{3}$$

where $K_{11}$, $K_{22}$ and $K_{33}$ are the elastic constants of splay, twist and bend distortion, respectively, and the unit vector $\mathbf{n}$ is the director of nematic liquid crystals. The elastic constants are functions of the order parameter and becomes zero in the isotropic phase. Here the electric field is considered as the external field and $f_e$ is given by [14, 15]

$$f_e = -\frac{1}{2}\varepsilon_0 \Delta\varepsilon(\mathbf{n} \cdot \mathbf{E})^2, \tag{4}$$

where $\Delta\varepsilon$ is the dielectric anisotropy of the liquid crystal, $\varepsilon_0$ is the dielectric constant of free space and $\mathbf{E}$ is the electric field. Here it is assumed that the electric field $\mathbf{E}$ is constant in a droplet, which neglects the distortion of the field due to the deformed director configuration. While this is a significant assumption, inclusion of an inhomogeneous field would considerably complicate the calculation. Furthermore it is not clear that it would be any closer to reality, since in the PDLC device inter-droplet interactions are likely to distort the field distribution just as much as intra-droplet inhomogeneities. The dielectric anisotropy of the liquid crystal $\Delta\varepsilon$ is a function of the order parameter and becomes zero in the isotropic phase.

It is assumed that directors prefer to align normal to the surface. The surface energy term is given by [5]

$$f_s = -\frac{1}{2}W_0\{(\mathbf{n} \cdot \mathbf{s})^2 - 1\}, \tag{5}$$

where $W_0$ is the anchoring strength and $\mathbf{s}$ is the surface normal unit vector.

In this paper, the droplet is treated as having rotational symmetry around the director of electric field $\mathbf{E}$ (see figure 1). Since we wish to consider both spherical and oblate droplets, it is convenient to use cylindrical coordinates $(r, \phi, z)$ in terms of which the equation of the surface takes the form

$$\left(\frac{r}{R}\right)^2 + \left(\frac{z}{\alpha R}\right)^2 = 1. \tag{6}$$

The conditions $\alpha = 1$ corresponds to a spherical droplet of radius $R$ and $\alpha < 1$ to an oblate droplet.

Equation (1) now becomes

$$\begin{aligned} F = & \int_{-\alpha R}^{\alpha R} \int_0^{(R^2-(z/\alpha)^2)^{1/2}} \int_0^{2\pi} f_b \, d\phi r \, dr \, dz \\ & + \int_{-\alpha R}^{\alpha R} \int_0^{2\pi} [f_s (r^2 + (z/\alpha^2)^2)^{1/2}]_{surf} \, d\phi \, dz \\ = & \, 2\pi K_{11} R \left[ \int_{-\alpha}^{\alpha} \int_0^{(1-(\zeta/\alpha)^2)^{1/2}} f_b/(K_{11}/R^2) \rho \, d\rho \, d\zeta \right. \\ & \left. + \int_{-\alpha}^{\alpha} [f_s/(K_{11}/R)(\rho^2 + (\zeta/\alpha^2)^2)^{1/2}]_{surf} \, d\zeta \right] \end{aligned} \quad (7)$$

with

$$\rho = r/R, \; \zeta = z/R. \quad (8)$$

Here $[\,]_{surf}$ means that the contents in the bracket are evaluated at the surface, and from equation (6) $\rho$ and $\zeta$ satisfy

$$\rho^2 + (\zeta/\alpha)^2 = 1. \quad (9)$$

We limit our discussion to cases without twist distortion and represent the director by

$$\mathbf{n} = \sin \psi \mathbf{e}_\rho + \cos \psi \mathbf{e}_\zeta, \quad (10)$$

where $\mathbf{e}_\rho$ and $\mathbf{e}_\zeta$ are the unit vectors of the cylindrical coordinates and $\psi(\rho, \zeta)$ is the angle between the director $\mathbf{n}$ and $\mathbf{e}_\zeta$ (see figure 1 (*a*)). Inclusion of a twist distortion would require the introduction of an additional variable and would have further complicated the computations.

Using equations (3), (4), (5) and (10) gives

$$\begin{aligned} f_d/(K_{11}/R^2) = & \frac{1}{2}(\cos^2 \psi + k_3 \sin^2 \psi)\psi_\rho^2 \\ & + \frac{1}{2}(\sin^2 \psi + k_3 \cos^2 \psi)\psi_\zeta^2 \\ & - (1 - k_3)\psi_\rho \psi_\zeta \sin \psi \cos \psi \\ & + \frac{1}{\rho}(\psi_\rho \cos \psi - \psi_\zeta \sin \psi) \sin \psi \\ & + \frac{1}{2\rho^2} \sin^2 \psi \end{aligned} \quad (11\,a)$$

with

$$k_3 = K_{33}/K_{11}, \quad (11\,b)$$

$$f_e/(K_{11}/R^2) = -\frac{1}{2}\left(\frac{R}{\xi}\right)^2 \cos^2 \psi, \quad (12\,a)$$

where

$$\xi = \left(\frac{K_{11}}{\varepsilon_0 \Delta\varepsilon}\right)^{1/2} \frac{1}{E} \quad (12\,b)$$

is the correlation length [14], and

$$\begin{aligned} f_s/(K_{11}/R) = & \frac{1}{2}\left(\frac{R}{d_e}\right) \frac{1}{\rho^2 + (\zeta/\alpha^2)^2} \\ & \times \{\rho \cos \psi - (\zeta/\alpha^2) \sin \psi\}^2 \end{aligned} \quad (13\,a)$$

where

$$d_e = K_{11}/W_0 \quad (13\,b)$$

is the extrapolation length [14]. In equations (11), (12) and (13), $\psi_\rho$ and $\psi_\zeta$ represent $\partial\psi/\partial\rho$ and $\partial\psi/\partial\zeta$, respectively.

The stable director configuration is found by minimizing the free energy of a droplet given by equation (7). This can be achieved by solving the corresponding Euler–Lagrange equation,

$$\rho \frac{\partial f_b}{\partial \psi} - \frac{\partial f_b}{\partial \psi_\rho} - \rho \frac{\partial}{\partial \rho}\left(\frac{\partial f_b}{\partial \psi_\rho}\right) - \rho \frac{\partial}{\partial \zeta}\left(\frac{\partial f_b}{\partial \psi_\zeta}\right) = 0 \quad (14)$$

with the boundary condition

$$\rho \frac{\partial f_b}{\partial \psi_\rho} + (\zeta/\alpha^2) \frac{\partial f_b}{\partial \psi_\zeta} + \frac{1}{R} \frac{\partial f_s}{\partial \psi} (\rho^2 + (\zeta/\alpha^2)^2)^{1/2} = 0. \quad (15)$$

Derivations of equations (14) and (15) are given in the appendix. Taking account of equations (2) and (9) and substituting equations (11), (12) and (13) into equations (14) and (15), we can obtain the following form of the Euler–Lagrange equation:

$$\begin{aligned} & \rho(\cos^2 \psi + k_3 \sin^2 \psi)\psi_{\rho\rho} + \rho(\sin^2 \psi + k_3 \cos^2 \psi)\psi_{\zeta\zeta} \\ & - \rho(1 - k_3)\psi_\rho \psi_\zeta \cos 2\psi \\ & - \frac{1}{2}(1 - k_3)(\psi_\rho^2 - \psi_\zeta^2 + 2\psi_{\rho\zeta}) \sin 2\psi \\ & + (\cos^2 \psi + k_3 \sin^2 \psi)\psi_\rho - \frac{1}{2}(1 - k_3)\psi_\zeta \sin 2\psi \\ & - \frac{1}{2\rho} \sin 2\psi - \frac{1}{2}\rho\left(\frac{R}{\xi}\right)^2 \sin 2\psi = 0 \end{aligned} \quad (16)$$

and the boundary condition

$$\rho\left\{(\cos^2\psi+k_3\sin^2\psi)\psi_\rho - \frac{1}{2}(1-k_3)\psi_\zeta\sin 2\psi+\frac{1}{2\rho}\sin 2\psi\right\} + (\zeta/\alpha^2)\left\{(\sin^2\psi+k_3\cos^2\psi)\psi_\zeta - \frac{1}{2}(1-k_3)\psi_\rho\sin 2\psi-\frac{1}{\rho}\sin^2\psi\right\} - \frac{1}{2}\left(\frac{R}{d_e}\right)\frac{1}{(\rho^2+(\zeta/\alpha^2)^2)^{1/2}} \times\{(\rho^2-(\zeta/\alpha^2)^2)\sin 2\psi+2\rho(\zeta/\alpha^2)\cos 2\psi\}=0. \tag{17}$$

Generally $k_3$ and $\xi$ are functions of the order parameter which decreases in the vicinity of the disclination due to the large distortion of the director configuration [6].

As a first approximation, we assume that $k_3$ is constant regardless of the order parameter. In this case equation (16) still depends on the order parameter through $\xi$ in the external field term. However the distortion terms are much larger than the external field term in the vicinity of the disclination and the order parameter is constant out of this region. Therefore the order parameter dependence is negligible in equation (16). The director configuration can be determined with a constant $k_3$ regardless of the order parameter.

In the numerical calculation of the director configurations, the disclination is fixed and the boundary surrounding the disclination region is defined as the disclination boundary. Here the distance from the disclination to the boundary is negligible in comparison with the droplet radius. The directors on this boundary are fixed while solving equations (16) and (17) numerically. Their values are determined by solving the Euler–Lagrange equation corresponding to the vicinity of the disclination where the external field term $f_e$ is negligible compared with the distortion term $f_d$. The three possible disclinations in a droplet with surface normal anchoring are (1) the disclination point at the centre of the droplet (at $\rho=\zeta=0$), (2) the circle disclination ring on the equator plane of the droplet (at $0<\rho<1$, $\zeta=0$), (3) the circle disclination ring on the equator (at $\rho=1$, $\zeta=0$).

For case (1), it is convenient to use the spherical coordinates $(r, \theta, \phi)$ with the point disclination at the origin and take

$$\mathbf{n}=\cos\upsilon\mathbf{e}_\rho-\sin\upsilon\mathbf{e}_\theta, \tag{18}$$

where $\rho=r/R$, $\mathbf{e}_\rho$ and $\mathbf{e}_\theta$ are the unit vectors of the spherical coordinates and $\upsilon(\rho,\theta)$ is the angle between the director $\mathbf{n}$ and $\mathbf{e}_\rho$ (see figure 1 (*b*)). The distortion free energy density $f_d$ is then given by

$$f_d/(K_{11}/R^2)=\frac{1}{2}\left\{\upsilon_\rho\sin\upsilon+\frac{1}{\rho}\upsilon_\theta\cos\upsilon+\frac{1}{\rho}(\cot\theta\sin\upsilon-2\cos\upsilon)\right\}^2 + \frac{1}{2}k_3\left\{\upsilon_\rho^2\cos^2\upsilon+\frac{1}{\rho^2}\upsilon_\theta^2\sin^2\upsilon+\frac{1}{\rho}\upsilon_\rho\sin 2\upsilon - \frac{2}{\rho^2}\upsilon_\theta\sin^2\upsilon-\frac{1}{\rho}\upsilon_\rho\upsilon_\theta\sin 2\upsilon+\frac{1}{\rho^2}\sin^2\upsilon\right\}. \tag{19}$$

Here $\upsilon_\rho$ and $\upsilon_\theta$ represent $\partial\upsilon/\partial\rho$ and $\partial\upsilon/\partial\theta$, respectively. The corresponding Euler–Lagrange equation is given by

$$(\sin^2\upsilon+k_3\cos^2\upsilon)\rho^2\sin\theta\upsilon_{\rho\rho}+(\cos^2\upsilon+k_3\sin^2\upsilon)\sin\theta\upsilon_{\theta\theta} - \frac{1}{2}(k_3-1)\sin\theta\sin 2\upsilon(\rho^2\upsilon_\rho^2-\upsilon_\theta^2) - (k_3-1)\rho\sin\theta(\upsilon_{\rho\theta}\sin 2\upsilon+\upsilon_\rho\upsilon_\theta\cos 2\upsilon) + \left\{2(\sin^2\upsilon+k_3\cos^2\upsilon)\sin\theta - \frac{1}{2}(k_3-1)\cos\theta\sin 2\upsilon\right\}\rho\upsilon_\rho + \left\{(\cos^2\upsilon+k_3\sin^2\upsilon)\cos\theta-\frac{1}{2}(k_3-1)\sin\theta\sin 2\upsilon\right\}\upsilon_\theta - \frac{1}{2}\frac{1}{\sin\theta}\sin 2\upsilon+\sin\theta\sin 2\upsilon-(1+k_3)\cos\theta\sin^2\upsilon=0. \tag{20}$$

As $\rho$ is very small on the disclination boundary, the terms containing $\rho$ are neglected and equation (20) approximated by

$$G(\upsilon)\left\{\upsilon_{\theta\theta}\sin^2\theta+\frac{1}{2}(\upsilon_\theta-1)\sin 2\theta\right\} + \frac{1}{2}\frac{\partial G(\upsilon)}{\partial\upsilon}(\upsilon_\theta-1)\upsilon_\theta\sin^2\theta-\frac{1}{2}\sin 2(\upsilon-\theta)=0 \tag{21 a}$$

with

$$G(\upsilon)=\cos^2\upsilon+k_3\sin^2\upsilon. \tag{21 b}$$

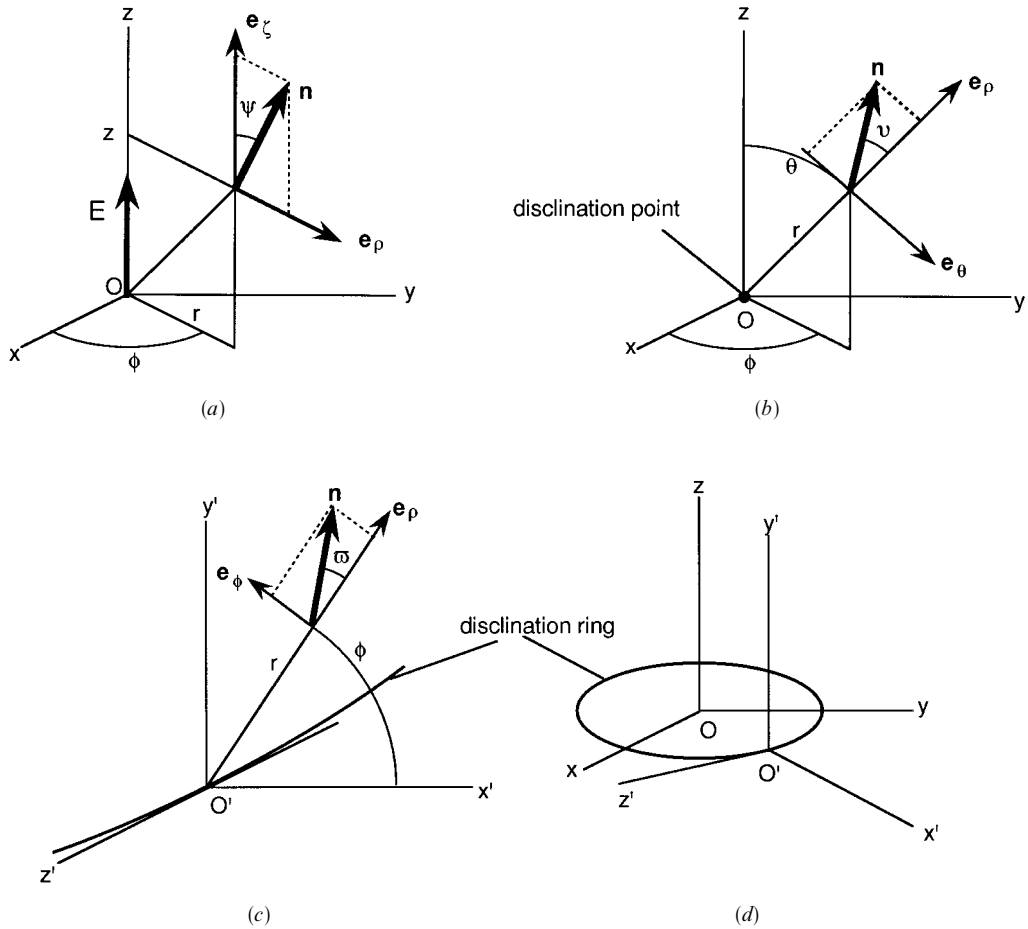


Figure 1. (*a*) Schematic presentation of the director **n** in the cylindrical coordinates. (*b*) Schematic presentation of the director **n** in the spherical coordinates. (*c*) and (*d*): Schematic presentation of the director **n** in the cylindrical coordinates where the $z'$ axis is everywhere tangential to the disclination ring.



This differential equation is solved subject to the conditions

$$\upsilon(\theta=0)=0, \tag{22a}$$

$$\upsilon(\theta=\pi/2)=0. \tag{22b}$$

Equations (22*a*) and (22*b*) follow from the symmetry with respect to the $Oxy$ plane and the $z$-axis in figure 1(*b*), respectively. Obviously $\upsilon=0$ satisfies equations (21) and (22), and so $\upsilon=0$ is taken as the fixed value on the disclination boundary for case (1). This corresponds to a zero-bend distortion.

For case (2) and (3), it is convenient to introduce local cylindrical coordinates $(r, \phi, z)$ where the $z$ axis is everywhere tangential to the disclination ring and take

$$\mathbf{n}=\cos\bar{\omega}\mathbf{e}_\rho+\sin\bar{\omega}\mathbf{e}_\phi, \tag{23}$$

where $\rho=r/R$, $\mathbf{e}_\rho$ and $\mathbf{e}_\theta$ are the unit vectors of the cylindrical coordinates and $\bar{\omega}(\rho, \phi)$ is the angle between the director **n** and $\mathbf{e}_\rho$ (see figure 1(*c*) and (*d*)). The $O'x'y'$ plane is always perpendicular to the $O'z'$ direction. The distortion free energy density is given by

$$f_d/(k_{11}/R^2)=\frac{1}{2}\left(\frac{1}{\rho}\cos\bar{\omega}-\bar{\omega}_\rho\sin\bar{\omega}+\frac{1}{\rho}\bar{\omega}_\phi\cos\bar{\omega}\right)^2+\frac{1}{2}k_3\left(\frac{1}{\rho}\sin\bar{\omega}+\bar{\omega}_\rho\cos\bar{\omega}+\frac{1}{\rho}\bar{\omega}_\phi\sin\bar{\omega}\right)^2 \tag{24}$$

Here $\bar{\omega}_\rho$ and $\bar{\omega}_\phi$ represent, $\partial\bar{\omega}/\partial\rho$ and $\partial\bar{\omega}/\partial\phi$, respectively. The corresponding Euler–Lagrange equation in the cylindrical coordinates is given by

$$\begin{aligned}&(\sin^2\bar{\omega}+k_3\cos^2\bar{\omega})\rho^2\bar{\omega}_{\rho\rho}+(\cos^2\bar{\omega}+k_3\sin^2\bar{\omega})\bar{\omega}_{\phi\phi}\\&-\frac{1}{2}(k_3-1)\sin 2\bar{\omega}(\rho^2\bar{\omega}_\rho^2-\bar{\omega}_\phi^2)\\&+(k_3-1)\rho(\bar{\omega}_{\rho\phi}\sin 2\bar{\omega}+2\bar{\omega}_\rho\bar{\omega}_\phi\cos 2\bar{\omega})\\&+(\sin^2\bar{\omega}+k_3\cos^2\bar{\omega})\rho\bar{\omega}_\rho-\frac{1}{2}(k_3-1)\sin 2\bar{\omega}=0.\end{aligned} \tag{25}$$

As $\rho$ is very small on the boundary, the terms containing $\rho$ are negligible. Therefore equation (25) can be approximated by

$$G(\bar{\omega})\bar{\omega}_{\phi\phi}+\frac{1}{2}\frac{\partial G(\bar{\omega})}{\partial\bar{\omega}}(\bar{\omega}_{\phi}^{2}-1)=0. \qquad (26)$$

The solution for case (2) is obtained by solving equation (26) numerically subject to the conditions,

$$\bar{\omega}(\phi=0)=0, \qquad (27\,a)$$

$$\bar{\omega}(\phi=2\pi)=-\pi. \qquad (27\,b)$$

These conditions follow from the symmetry with respect to the $O'x'z'$ plane in figures 1 (*c*) and (*d*) and the strength of the disclination which is 1/2.

For case (3) equation (26) is solved subject to the conditions,

$$\bar{\omega}(\phi=\pi/2)=-\pi/2, \qquad (28\,a)$$

$$\bar{\omega}(\phi=\pi)=-\pi/2. \qquad (28\,b)$$

These conditions follow from the symmetry with respect to the $O'x'z'$ plane in figures 1 (*c*) and (*d*), and the surface normal boundary condition at the droplet surface. In this case $\bar{\omega}=-\pi/2$ satisfies equations (26) and (28), and so this is used as the fixed value on the boundary surrounding the disclination ring on the surface. This corresponds to a zero-splay distortion.

The director configurations for the fixed disclinations in a droplet outside the disclination region are obtained by solving equation (16) with the boundary condition equation (17) and the fixed values on the disclination boundary.

In order to find the stable state, the free energies of a droplet are calculated for each director configuration which are obtained with respect to the fixed disclination. By comparing each free energy, the stable director



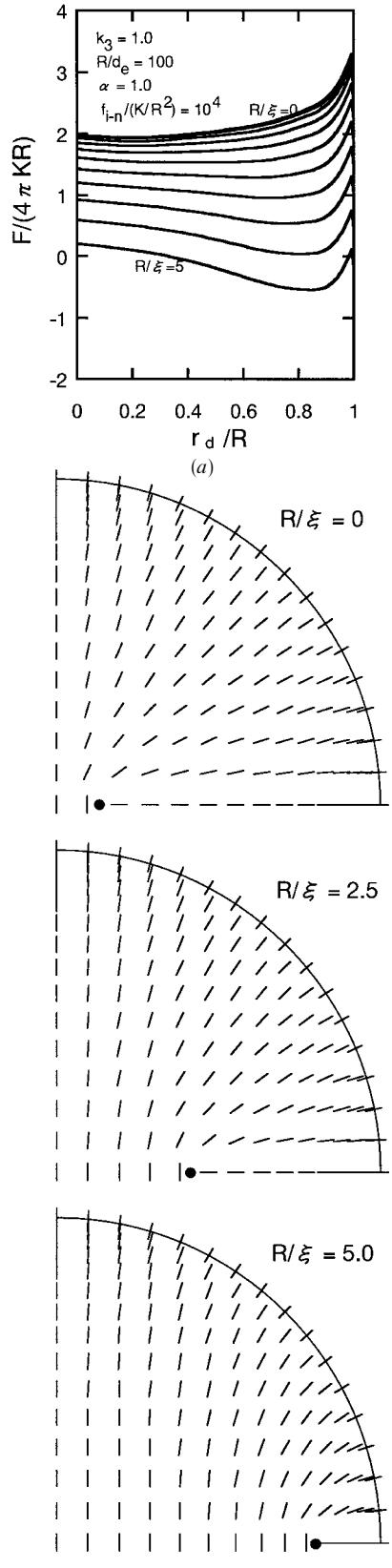


Figure 2.

Figure 2. (*a*) Free energy of a spherical droplet as a function of $r_d$ for $R/\xi=0$ to 5·0 with $K_{33}/K_{11}=1{\cdot}0$, $R/d_e=100$ and $f_{i-n}/(K/R^2)=10^4$. (*b*) Director configurations of a spherical droplet for $R/\xi=0$, 2·5, 5·0 with $K_{33}/K_{11}=1{\cdot}0$, $R/d_e=100$ and $f_{i-n}/(K/R^2)=10^4$.

Figure 3. (*a*) Free energy of a spherical droplet as a function of $r_d$ for $R/\xi=0$ to 5·0 with $K_{33}/K_{11}=1{\cdot}0$, $R/d_e=100$ and $f_{i-n}/(K/R^2)=10^2$. (*b*) Director configurations of a spherical droplet for $R/\xi=0$, 2·5, 5·0 with $K_{33}/K_{11}=1{\cdot}0$, $R/d_e=100$ and $f_{i-n}/(K/R^2)=10^2$.

Figure 4. (*a*) Free energy of a spherical droplet as a function of $r_d$ for $R/\xi=0$ to 5·0 with $K_{33}/K_{11}=1{\cdot}0$, $R/d_e=100$ and $f_{i-n}/(K/R^2)=10^6$. (*b*) Director configurations of a spherical droplet for $R/\xi=0$, 2·5, 5·0 with $K_{33}/K_{11}=1{\cdot}0$, $R/d_e=100$ and $f_{i-n}/(K/R^2)=10^6$.

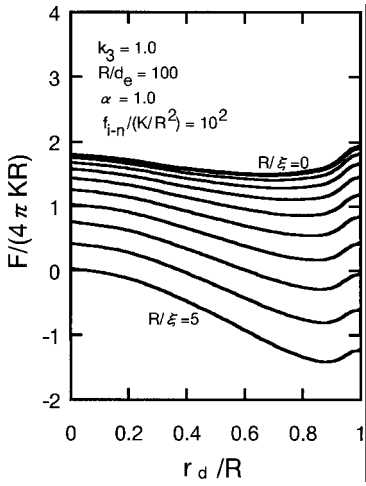


(*a*)

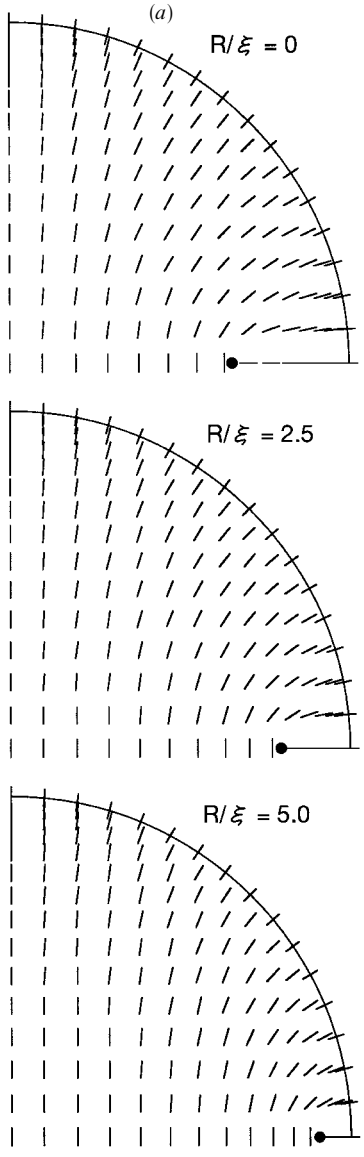


(*b*)

Figure 3.

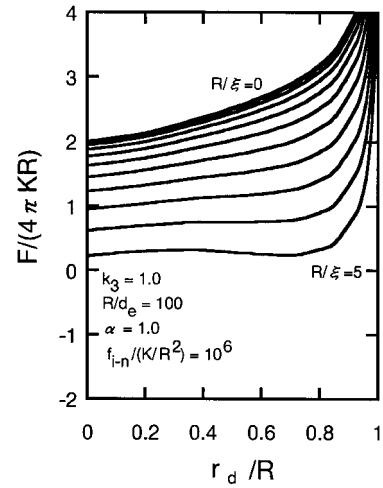


(*a*)

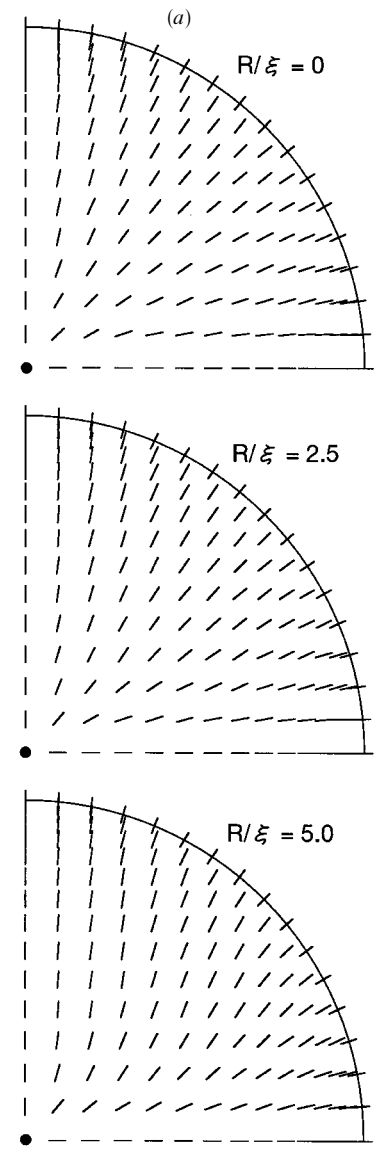


(*b*)

Figure 4.

configuration can be found by minimizing the free energy of a droplet. In the calculation of the free energy the order parameter is assumed to be constant in the droplet except in the vicinity of the disclination. The free energy density of the nematic phase cannot exceed the free energy density of the isotropic phase $f_i$, so that the large distortion term in the vicinity of the disclination causes the nematic–isotropic transition and the order parameter becomes zero. In this region the free energy density is defined to be equal to $f_i$.

Based on the Landau–de Gennes theory, the difference between the isotropic free energy density and the nematic free energy density without distortion can be written in terms of the order parameter $S$ [14] as

$$f_i - f_n = -\frac{1}{2}a(T - T_c^*)S^2 + \frac{1}{3}bS^3 - \frac{1}{4}cS^4. \quad (29)$$

By using the values of a common nematic liquid crystal 5CB [$a = 0{\cdot}1319 \times 10^6$ Jm$^{-3}$ K$^{-1}$, $b = 1{\cdot}836 \times 10^6$ Jm$^{-3}$, $c = 4{\cdot}050 \times 10^6$ Jm$^{-3}$] and $S = 0{\cdot}6$, $T - T_c^* = -10$ K, $f_i - f_n$ becomes of the order of $10^5$. Taking the radius of a droplet $R = 1$ μm and a typical elastic constant to be $10^{-11}$ N, the dimensionless parameter corresponding to the difference between an isotropic and a nematic free energy density, $(f_i - f_n)/(K/R^2) = f_{i-n}/(K/R^2)$ with $K = (K_{11} + K_{33})/2$, becomes of the order of $10^4$. We use $f_{i-n}/(K/R^2) = 10^4$ as a typical value in the following discussion.

The numerical calculation of the free energies of a droplet are performed by employing the following procedure. The droplet is subdivided into a mesh, and the directors at each mesh point are determined numerically by means of finite difference solutions of equation (16) subject to the boundary condition equation (17) and the fixed boundary conditions on the disclination boundary. The Newton–Raphson method is employed to solve the resulting system of non-linear finite difference equations. Then each mesh is subdivided into a finer mesh and the initial estimates of the directors at each mesh point in the finer mesh are determined by interpolation from the calculated results for the coarser mesh. These estimates are used to obtain more accurate approximation of the free energy densities at each point within the finer mesh. If the free energy density given by equation (2) exceeds the defined isotropic free energy density, then the former is reset to be the same as the latter. In these calculations, the results depend on the mesh size. The process of mesh refinement is continued until there is negligible change

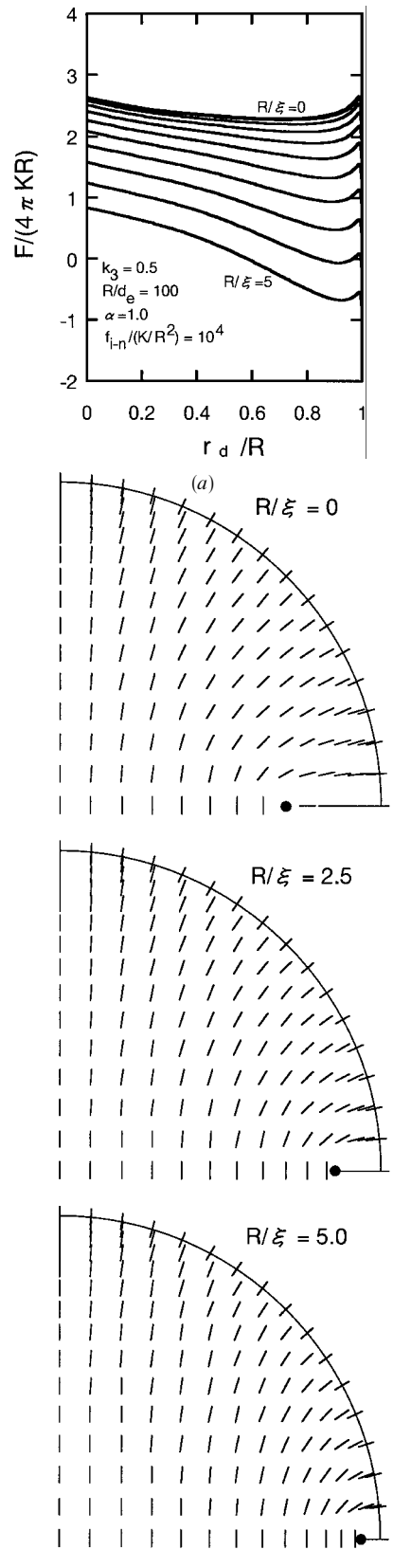


Figure 5. (*a*) Free energy of a spherical droplet as a function of $r_d$ for $R/\xi = 0$ to 5·0 with $K_{33}/K_{11} = 0{\cdot}5$, $R/d_e = 100$ and $f_{i-n}/(K/R^2) = 10^4$. (*b*) Director configurations of a spherical droplet for $R/\xi = 0$, 2·5, 5·0 with $K_{33}/K_{11} = 0{\cdot}5$, $R/d_e = 100$ and $f_{i-n}/(K/R^2) = 10^4$

in the total free energy of the droplet as the mesh size is further reduced. The accuracy of the numerical solution of equation (16) and the calculated free energy of the droplet are improved by means of refinement of the mesh size which is initially used in solving equation (16). Details of the finite difference schemes approximating equations (16) and (17), together with the Newton–Raphson procedure, and the procedure for obtaining the free energy of the droplet will be presented elsewhere [16].

## 3. Results

In the following discussion, 'radial structure' is used for the structure with the equatorial disclination ring near the centre of the droplet as well as the structure with the point disclination at the centre. In the same way, 'axial structure' is used for the structure with the disclination ring apart from the centre as well as the structure with the disclination ring on the surface. Here $r_d$ is defined as the distance from the centre of a droplet to the equatorial disclination ring, i.e. the radius of the disclination ring.

Figure 2 (*a*) shows the free energy of a droplet as a function of $r_d$ for $R/\xi = 0$ to 5 with $\alpha = 1$ (spherical droplet), $k_3 = 1$, $R/d_e = 100$ and $f_{i-n}/(K/R^2) = 10^4$. $R$ is the radius of a droplet and $k = (K_{11} + K_{33})/2$. The dimensionless parameter $R/d_e = 100$ corresponds to the strong anchoring strength. The value of $r_d$ which gives the minimum value of the free energy corresponds to the radius of the disclination ring in the stable state. Figure 2 (*b*) shows the stable director configuration which gives the minimum free energy for $R/\xi = 0$, 2·5, 5. The disclination ring exists close to the centre of the droplet for the low applied field $R/\xi$. With increasing the field, the disclination ring expands outward and it exists close to the surface for the high applied field, i.e. the radial to axial structure transition occurs.

Figures 3 (*a*) and 4 (*a*) show the free energy of a droplet with $f_{i-n}/(K/R^2) = 10^2$ and $f_{i-n}/(K/R^2) = 10^6$, respectively. The other parameters are the same as those in figure 2. Figures 3 (*b*) and 4 (*b*) show the stable director configurations corresponding to figures 3 (*a*) and 4 (*a*), respectively. The case $f_{i-n}/(K/R^2) = 10^2$ corresponds to a smaller droplet (~0·1 μm) or higher temperature and the case $f_{i-n}/(K/R^2) = 10^6$ to a larger droplet (~10 μm). When $f_{i-n}/(K/R^2)$ is small ($= 10^2$), the minimum value of the free energy occurs at the large value of $r_d$ regardless of the applied field, i.e. the axial structure is stable. On

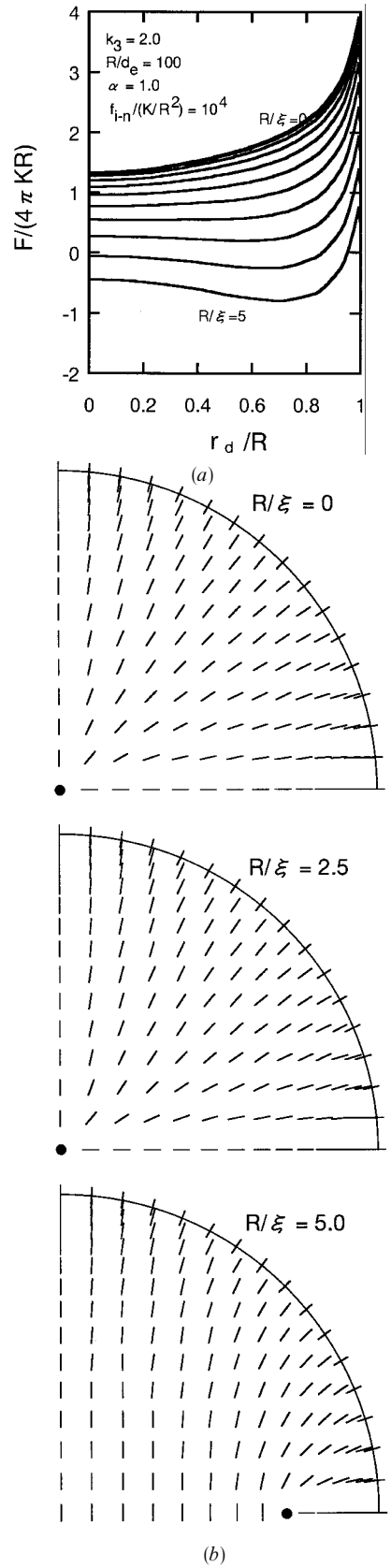


Figure 6. (*a*) Free energy of a spherical droplet as a function of $r_d$ for $R/\xi = 0$ to 5·0 with $K_{33}/K_{11} = 2{\cdot}0$, $R/d_e = 100$ and $f_{i-n}/(K/R^2) = 10^4$. (*b*) Director configurations of a spherical droplet for $R/\xi = 0$, 2·5, 5·0 with $K_{33}/K_{11} = 2{\cdot}0$, $R/d_e = 100$ and $f_{i-n}/(K/R^2) = 10^4$.

the other hand, when $f_{i-n}/(K/R^2)$ is large ($=10^6$), the free energy increases rapidly with increasing $r_d$, so that the radial structure is stable. In our assumption the disclination ring consists of an isotropic core which has the isotropic free energy density. The length of the disclination ring increases with increasing $r_d$. Therefore if the isotropic free energy density is large, the free energy associated with the disclination ring becomes large rapidly with increasing $r_d$ and the total free energy of a droplet becomes very large. In this case the point disclination is still stable at the high applied field $R/\xi = 5$ although there is a large distortion in the director configuration as is shown in figure 4 (*b*).

Figures 5 (*a*) and 6 (*a*) show the free energy of a droplet when a bend elastic constant is smaller than a splay elastic constant, $K_{33}/K_{11} = k_3 = 0{\cdot}5$ and larger than it, $K_{33}/K_{11} = k_3 = 2{\cdot}0$, respectively. The other parameters are the same as those in figure 2. Figures 5 (*b*) and 6 (*b*) show the stable director configurations corresponding to figures 5 (*a*) and 6 (*a*), respectively. When $K_{33}$ is smaller than $K_{11}$, the axial structure is stable. On the other hand, if $K_{33}$ is larger than $K_{11}$, the point disclination exists at the centre of a droplet with the small applied field. However with increasing the field, the point disclination becomes a disclination ring and expands suddenly toward the surface at the critical applied field; there is a first-order transition from the radial to axial structure. The stability of the radial structure with large bend elastic constant can be explained as follows. The transition from the radial to the axial structure is accompanied by the bend distortion and the large bend elastic constant prevents this distortion: the radial structure is stable in this case.

Figure 7 (*a*) shows the free energy of an oblate droplet, i.e. $\alpha = 0{\cdot}5$. The other parameters are the same as those in figure 2. Figure 7 (*b*) shows the stable director configurations corresponding to figure 7 (*a*). In this case the axial structure is stable regardless of the applied field. The director configurations show almost no change with respect to the applied field as is shown in figure 7 (*b*).

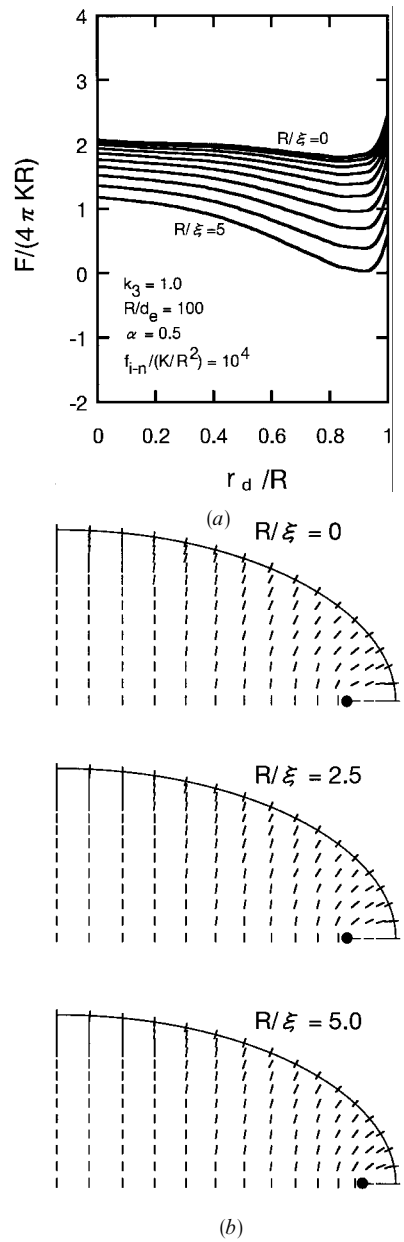


Figure 7. (*a*) Free energy of an oblate droplet ($\alpha = 0{\cdot}5$) as a function of $r_d$ for $R/\xi = 0$ to 5·0 with $K_{33}/K_{11} = 1{\cdot}0$, $R/d_e = 100$ and $f_{i-n}/(K/R^2) = 10^4$. (*b*) Director configurations of an oblate droplet ($\alpha = 0{\cdot}5$) for $R/\xi = 0$, 2·5 5·0 with $K_{33}/K_{11} = 1{\cdot}0$, $R/d_e = 100$ and $f_{i-n}/(K/R^2) = 10^4$.

## 4. Conclusions

The radial–axial structure transitions of a spherical and oblate droplet with a surface normal anchoring condition have been calculated with the following assumptions. (1) The ratio of elastic constants, $K_{33}/K_{11}$ is constant in a droplet even in the vicinity of the disclination. (2) Large distortions around the disclination cause the nematic–isotropic phase transition, so that the disclination core is isotropic.

The following results were obtained from these calculations: (1) The radial structure is stable for a low applied field and the axial structure is stable for a high applied field. (2) When the difference between the isotropic free energy density and the nematic free energy density without distortion, $f_{i-n}$, is large, the radial structure is stable. On the other hand, when $f_{i-n}$ is small, the axial structure is stable. (3) When $K_{33}$ is larger than $K_{11}$, the radial structure is stable and the 1st order transition occurs from the radial structure to the axial structure with increasing applied field. On the other hand, when $K_{33}$ is smaller than $K_{11}$, the axial structure is stable. (4) In an oblate droplet, the axial structure is

stable and the director configurations show almost no change with respect to the applied field.

## Appendix

The Euler–Lagrange equations (14) and (15) are derived as follows. From equation (7) the variation of the free energy $\delta F$ due to $\delta\psi$ is represented by

$$\delta F = 2\pi R^3 \int_{-\alpha}^{\alpha}\int_{0}^{1-(\zeta/\alpha)^2} \times \left[\frac{\partial f_b}{\partial \psi}\partial\psi + \frac{\partial f_b}{\partial \psi_\rho}(\delta\psi)_\rho + \frac{\partial f_b}{\partial \psi_\zeta}(\delta\psi)_\zeta\right]\rho\,\mathrm{d}\rho\,\mathrm{d}\zeta + 2\pi R^2 \int_{-\alpha}^{\alpha}\left[\frac{\partial f_s}{\partial \psi}\partial\psi(\rho^2+(\zeta/\alpha^2)^2)^{1/2}\right]_{surf}\mathrm{d}\zeta. \quad (A1)$$

Using the following expressions,

$$\left(\frac{\partial f_b}{\partial \psi_\rho}(\delta\psi)_\rho\right)\rho = \left\{\frac{\partial}{\partial\rho}\left(\frac{\partial f_b}{\partial\psi_\rho}\delta\psi\right) - \frac{\partial}{\partial\rho}\left(\frac{\partial f_b}{\partial\psi_\rho}\right)\delta\psi\right\}\rho = \frac{\partial}{\partial\rho}\left(\rho\frac{\partial f_b}{\partial\psi_\rho}\delta\psi\right) - \frac{\partial f_b}{\partial\psi_\rho}\delta\psi - \rho\frac{\partial}{\partial\rho}\left(\frac{\partial f_b}{\partial\psi_\rho}\right)\delta\psi \quad (A2\,a)$$

$$\left(\frac{\partial f_b}{\partial \psi_\zeta}(\delta\psi)_\zeta\right)\rho = \left\{\frac{\partial}{\partial\zeta}\left(\frac{\partial f_b}{\partial\psi_\zeta}\delta\psi\right) - \frac{\partial}{\partial\zeta}\left(\frac{\partial f_b}{\partial\psi_\zeta}\right)\delta\psi\right\}\rho = \frac{\partial}{\partial\zeta}\left(\rho\frac{\partial f_b}{\partial\psi_\zeta}\delta\psi\right) - \rho\frac{\partial}{\partial\zeta}\left(\frac{\partial f_b}{\partial\psi_\zeta}\right)\delta\psi. \quad (A2\,b)$$

Equation (A1) is represented in the following form after some arrangements:

$$\delta F = 2\pi R^3 \int_{-\alpha}^{\alpha}\int_{0}^{(1-(\zeta/\alpha)^2)^{1/2}}\left[\rho\frac{\partial f_b}{\partial\psi} - \frac{\partial f_b}{\partial\psi_\rho} - \rho\frac{\partial}{\partial\rho}\left(\frac{\partial f_b}{\partial\psi_\rho}\right) - \rho\frac{\partial}{\partial\zeta}\left(\frac{\partial f_b}{\partial\psi_\zeta}\right)\right]\delta\psi\,\mathrm{d}\rho\,\mathrm{d}\zeta + 2\pi R^3\int_{-\alpha}^{\alpha}\left[\left\{\rho\frac{\partial f_b}{\partial\psi_\rho} + (\zeta/\alpha^2)\frac{\partial f_b}{\partial\psi_\zeta} + \frac{1}{R}\frac{\partial f_s}{\partial\psi}(\rho^2+(\zeta/\alpha^2)^2\right\}\delta\psi\right]_{surf}\mathrm{d}\zeta. \quad (A3)$$

In order to achieve $\delta F = 0$ regardless of $\delta\psi$, the following equations must be satisfied:

$$\rho\frac{\partial f_b}{\partial\psi} - \frac{\partial f_b}{\partial\psi_\rho} - \rho\frac{\partial}{\partial\rho}\left(\frac{\partial f_b}{\partial\psi_\rho}\right) - \rho\frac{\partial}{\partial\zeta}\left(\frac{\partial \hat{f}_b}{\partial\psi_\zeta}\right) = 0 \quad (14)$$

$$\rho\frac{\partial f_b}{\partial\psi_\rho} + (\zeta/\alpha^2)\frac{\partial f_b}{\partial\psi_\zeta} + \frac{1}{R}\frac{\partial f_s}{\partial\psi}(\rho^2+(\zeta/\alpha^2)^2)^{1/2} = 0. \quad (15)$$

## References


[1] Zumer, S., 1988, *Phys. Rev. A*, **37,** 4006.
[2] Drzaic, P. S., 1988, *Liq. Cryst.*, **3,** 1543.
[3] Bondar, V. G., Lavrentovich, O. D., and Pergamenschchik, V. M., 1992, *Sov. Phys. JETP*, **74,** 60.
[4] Kralj, S., and Zumer, S., 1992, *Phys. Rev. A*, **45,** 2461.
[5] Zumer, S., Kralj, S., and Bezic, J., 1992, *Mol. Cryst. liq. Cryst.*, **212,** 163.
[6] Kralj, S., Zumer, S., and Allender, D. W., 1991, *Phys. Rev. A*, **43,** 2943.
[7] Fergason, J. L., 1985, *SID Technical Digest*, **16,** 68.
[8] Drzaic, P., 1986, *J. appl. Phys.*, **60,** 2142.
[9] Doane, J. W., Vaz, N. A., Wu, B.-G., and Zumer, S., 1986, *Appl. Phys. Lett.*, **48,** 269.
[10] Doane, J. W., Golemme, A., West, J. L., Whitehead, Jr., J. B., and Wu, B.-G., 1988, *Mol. Cryst. liq. Cryst.*, **165,** 511.
[11] Hirai, Y., Niiyama, S., Ooi, Y., Kunigita, M., and Kumai, H., 1991, *SID'91 Digest*, 594.
[12] Ooi, Y., Sekine, M., S. Niiyama, Hirai, Y., Kunigita, M., Wakabayashi, T., Yuki, M., and Gunjima, T., 1992, *Japan Display '92 Proc.*, 113.
[13] Jones, P., Tomita, A., and Wartenberg, W., 1991, *Proc. SPIE*, **1456,** 6.
[14] de Gennes, P. G., and Prost, J., 1993, *Physics of Liquid Crystals* (Clarendon Press, Oxford).
[15] Vertogen, G., and de Jeu, W. H., 1988, *Thermotropic Liquid Crystals* (Springer-Verlag, Heidelberg).
[16] Komura, S., Atkin, R. J., Stern, M. S., and Dunmur, D. A. (to be published).